A Simple Model for Small Collections of Magnetic Plasmonic Oligomers

Nicholas P. Montoni,[†] Steven C. Quillin,[†] Charles Cherqui,[†] and David J. Masiello[*,†,‡]

†*Department of Chemistry, University of Washington, Seattle, WA 98195*

‡*Department of Applied Mathematics, University of Washington, Seattle, WA 98195*

E-mail: masiello@chem.washington.edu

Abstract

Ring-like assemblies of metal nanoparticles that exhibit magnetic resonances, called magentic plasmon oligomers, have been of recent interest as negative-index metamaterials. Magnetic plasmon oligomers have potential applications in cloaking, superlensing, information transmission, and sensing. For these reasons, it is imperative to understand the properties of such systems on both small and large scales. We show through theory and simulation that the energy ordering of the magnetic resonances of small oligomers depends greatly on the size and scale of the nanoparticle assembly in ways that purely electric plasmons do not. Following this, we determine the effective pemeability and permittivity of periodic arrays of nanoparticles and show that in certain size regimes they exhibit a negative index of refraction at optical frequencies. As a final exercise, we propose a negative-index material composed of charge tunable semiconductor quantum dots to emphasize the direct control of the optical properties of 2-D magnetic materials.

Keywords

plasmon, hybridization, magnetic, retardation

1 Introduction

Metal nanoparticles (MNPs) support collective resonances of thier conductions electrons at optical frequencies. These localized surface plasmon resonances (LSPRs) can interact with each other in assemblies of two or more MNPs to produce hybridized resonances of the assembly, much like the hybridization of atomic orbitals in molecules. When these assemblies are arranged in rings, the single LSPRs can give rise to a fictitious, oscillating current which produces an oscillating magnetic dipole inside of the ring. Such systems are known as magnetic plasmon oligomers.

Magnetic plasmon oligomers have been of intense focus do to their potential applications in sensing, lensing, cloaking, and information processing. In a recent paper, Engheta *et al.* state that magnetic systems are well-understood on the single oligomer scale and the nearly infinite scale. [**CITE Engheta 2017**] However, the properties of collections of few magnetic oligomers have not been fully explored. Much work has been done to elucidate the properties of long chains and large arrays of magnetic oligomers. [**lots of Halas cites, probably**] The work of Cherqui *et al.* has shown the properties of magnetic systems comprising one, two, and six rings. Furthermore, the dependence of the magnetic properties of the systems on individual nanoparticle geometry, and the relative size of the constituent oligomers has also been determined. This formative work has explained much of the physics behind magnetic plasmons, but it has also raised an interesting problem.

In Cherqui's 2014 work on magnetic plasmons, a quasistatic, electric dipole tight-binding model was used to determine the eigenmodes of the magnetic systems. This model maps each considered only the electric near-field of the single-particle plasmons and only incorporated nearest-neighbor interactions. For one-ring systems, hereafter called monomers, the lowest

energy eigenmode was determined to be the magnetic mode. For the two-ring system, called a twomer, the lowest- and second-lowest-energy modes were determined to be an out-of-phase magnetic mode and an in-phase magnetic mode, respectively. However, in confiring their results with full-wave simulations, they found a discrepancy. While the tight-binding model accurately described the eigenmodes, it inaccurately described their energy-ordering. The simulations placed the in-phase magnetic mode lower in energy than the out-of-phase mode, opposite the ordering of the tight-binding model. An explanation was needed to determine why this result, while counterintuitive, was in fact physical. In this paper, we show that this apparent discrepancy is not only expected, but is rectifiable through expanding the tight-binding model to include all inter-particle interactions and the fully retarded electric field. Furthermore, we show that for small, multi-oligomer systems, the size, spacing, and environment greatyly impact the eigenspectrum and the ordering of magnetic modes, leading to a high degree of tunability. Finally, we recommend ways that this tunability might be enhanced and exploited in future studies.

Bringing two or more metal nanoparticles (MNPs) together allows their individual electric plasmons to hybridize, producing a new set of plasmonic modes.[1–4] Plasmon hybridization theory is applied to aggregates of MNPs and explains their collective behavior within the quasistatic limit in which the speed of light is taken to be infinite.[5–8] Recently, retardation effects on plasmon hybridization have been the focus of study for large particles[9,10] as well as dimers,[11–13] and 2-D arrays[14–16] of nanoparticles. Specific arrangements of nanoparticles in 2-D arrays, such as three or more nanoparticles arranged on the vertices of a regular polygon, support a collective mode in which all of the dipole plasmons are oriented head-to-tail. This generates a fictitious, oscillating current loop resulting in an oscillating magnetic dipole moment in the center of the ring.[17–22] These so-called magnetic plasmons are the lowest-energy collective modes of the oligomers and couple to and enhance the magnetic field of incident light,[23–25] offering a route to applications such as solar cell enhancement,[26–28] biosensing and detection,[29–36] and information storage and propagation.[37–39] The rich plasmonic modes of

magnetic-plasmon-supporting systems are well-described using plasmon hybridization theory, but when in the quasistatic limit, the energy-order of the modes is not.

Plasmon hybridization theory treats plasmons as point dipoles centered on their associated nanoparticles that interact through dipole-dipole coupling. In the quasistatic limit, these dipoles couple only through time-independent, electric near-field interactions,[40] but when the size of and distance between nanoparticles becomes large, this approximation breaks down and intermediate- and far-field effects must be considered, as well as time-delay effects in the near-field.[40] The aim of this paper is to incorporate the fully retarded electric field into plasmon hybridization theory and extend studies of retardation effects to magnetic plasmon oligomers. Specifically, we begin by exploring oligomers comprising two and three rings of nanoparticles and compare to full-wave simulation[41] to verify that our approach qualitatively predicts the energy-ordering of the magnetic modes.[21,22] Following this, we calaculate the coupling betwen individual rings in various oligomers in order to parametrize an effective magnetic-magnetic coupling between magnetic dipoles. Using this new basis, we describe periodic chains and arrays of oligomers.

The calculations presented here are performed using an electric tight-binding model, parametrizing the magnetic couplings, and then introducing these coupling constants into a magnetic tight-binding model. For all following magnetic oligomers, only the two planar dipoles per particle are considered in the electric tight binding model. The dipoles are mapped onto a set of harmonic oscillators and are described by the following Hamiltonian:

$$H = \sum_{i}^{n} \frac{\mathbf{P}_i^2}{2m_{\mathrm{sp},i}} + \frac{1}{2} m_{\mathrm{sp},i} w_{\mathrm{sp},i}^2 \mathbf{X}_i^2 + e^2 \sum_{i \neq j} \mathbf{X}_i \cdot \mathbf{\Lambda}_{\mathrm{full},ij} \cdot \mathbf{X}_j, \tag{1}$$

where $\mathbf{P}_i$ are the momenta conjugate to the coordinates $\mathbf{X}_i$, $\omega_{sp,i}$ are the individual LSPR frequencies of each oscillator, $m_{sp,i}$ are the LSPR effective masses and $\mathbf{\Lambda}_{\mathrm{full},ij}$ is the fully retarded dipole-dipole relay tensor (expanded below). To make this Hamiltonian more manageable, it is nondimensionalized using $\mathbf{Q}_i = (m_{\mathrm{sp}}\omega_{\mathrm{sp}}/\hbar)^{\frac{1}{2}}\, \mathbf{X}_i$ and $\mathbf{\Pi}_i = \mathbf{P}_i/\sqrt{\hbar m_{\mathrm{sp}}\omega_{\mathrm{sp}}}$. Substituting into Equation 1 and expanding $\mathbf{\Lambda}_{\mathrm{full},ij}$, we get:

$$H = \frac{\hbar\omega_{sp}}{2}\sum_{i}^{n}[\mathbf{\Pi}_i^2 + \mathbf{Q}_i^2] - \frac{\hbar\omega_{sp}}{2}\sum_{i\neq j}\{g_{ij}^{\mathrm{NF}}\left[3(\mathbf{Q}_i\cdot\hat{\mathbf{n}}_{ij})(\hat{\mathbf{n}}_{ij}\cdot\mathbf{Q}_j) - \mathbf{Q}_i\cdot\mathbf{Q}_j\right] + g_{ij}^{\mathrm{IF}}\left[3(\mathbf{Q}_i\cdot\hat{\mathbf{n}}_{ij})(\hat{\mathbf{n}}_{ij}\cdot\mathbf{Q}_j) - \mathbf{Q}_i\cdot\mathbf{Q}_j\right] - g_{ij}^{\mathrm{FF}}\left[(\mathbf{Q}_i\cdot\hat{\mathbf{n}}_{ij})(\hat{\mathbf{n}}_{ij}\cdot\mathbf{Q}_j) - \mathbf{Q}_i\cdot\mathbf{Q}_j\right]\}, \tag{2}$$

In this Hamiltonian we introduce the near, intermediate, and far-field coupling terms: $g_{ij}^{\mathrm{NF}} = \frac{\alpha_{sp}}{r_{ij}^3}\cos\left(\frac{\omega r_{ij}}{c}\right)$, $g_{ij}^{\mathrm{IF}} = \frac{\alpha_{sp}\omega}{r_{ij}^2 c}\sin\left(\frac{\omega r_{ij}}{c}\right)$, and $g_{ij}^{\mathrm{FF}} = \frac{\alpha_{sp}\omega^2}{r_{ij}c^2}\cos\left(\frac{\omega r_{ij}}{c}\right)$, respectively. Additionally, the polarizability $\alpha_{sp} = \frac{e^2}{m_{sp}\omega_{sp}^2}$, r_{ij} is the distance between the ith and jth LSPs, and $\hat{\mathbf{n}}_{ij}$ is the unit vector connecting two LSPs. Including these terms, we have incorporated all retardation effects associated with point dipoles.[42]

It should be noted that this Hamiltonian, when diagonilzed, results in a transcendental equation. The eigenvalues of the Hamiltonian are functions of ω, which are the frequencies of the collective modes, that is, the eigenvalues of the eigenvectors. In order to fully solve this problem, we make a first guess of ω for a particular mode of interest and iteratively compute the eigenvalues. Using the eigenvalue associated with the mode of interest, the Hamiltonian is diagonalized to convergence. The process is repeated for each mode of interest.

2 results and discussion

The first systems we examine are a magnetic two-mer,[21] three-mer chain, and three-mer triangle. Because we are interested in the effects of scale, we must define a scaling parameter for the system. Each of our systems begins from a unit cell called the one-mer: six silver, spherical MNPs placed at the corners of a regular hexagon. To create the two-mer, two unit cells are tiled so that they share an edge, and thus two particles. In general, if any two unit cells share an edge, they also share two nanoparticles, as in the diagrams in Figure **??** Each particle has radius a_0 and particles are separated by lattice spacing $r = 2.2 \times a_0$. With the radius of the particles defining the scale of the system, there now exists a way to probe the energy ordering of the modes as a function of size.

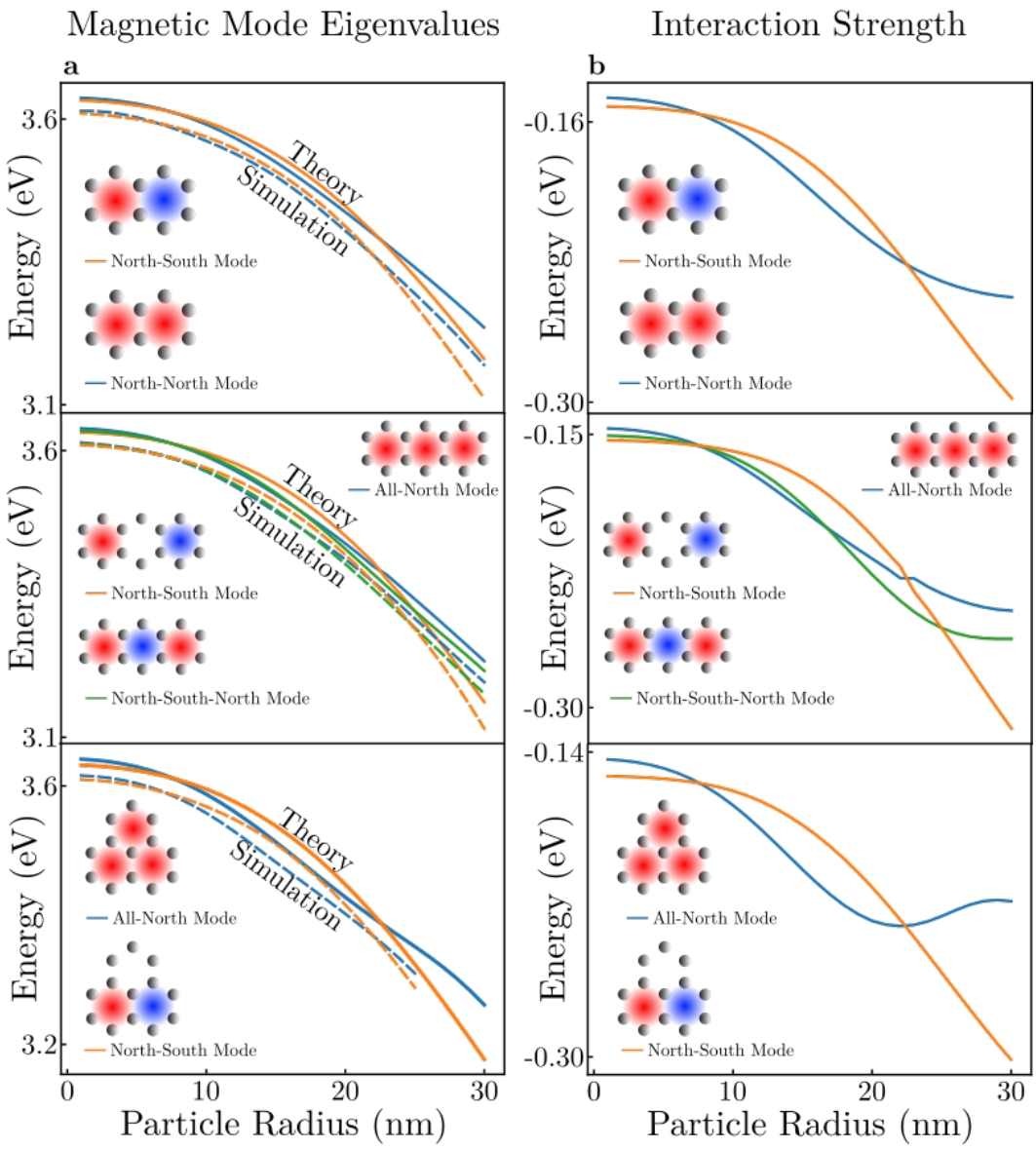

Figure 1: Magnetic mode eigenvalues (column a), predicted and simulated, and interaction strengths (column b) for the magnetic twomer (first row), threemer chain (second row), and threemer ring (thir d row). All of the magnetic modes range from 3.6 eV to 3.1 eV. In each system, the magnetic modes exhibit multiple crossings, showing that the eigenspectrum of these magnetic systems depends on th eir scale. The model consistently overestimates the eigenvalues by 0.5 eV, and consistently underes timates the crossing points by less than a nanometer. The twomer has two magnetic modes, one in-pha se mode (blue trace) and one out-of-phase mode (orange trace). The threemer chain has three modes, an in-phase mode (blue trace), a minimally out-of-phase mode (orange trace), and a maximally out-of -phase mode (green trace). The threemer ring exhibits three magnetic modes, but the out-of-phase mo des (orange trace) are degenerate so only one is depicted. The other mode is a maximally in-phase m ode (blue trace). To further emphasize the impact of scale, we have plotted the total interaction s trength of each eigenmode, *i.e.* the sum of each eigenvector's dot product with the electri c field of all of the other dipoles. This calculation reaffirms the scale dependence and predicts m ode crossings at the same scale as both the eigenvalue calculation and the simulations.

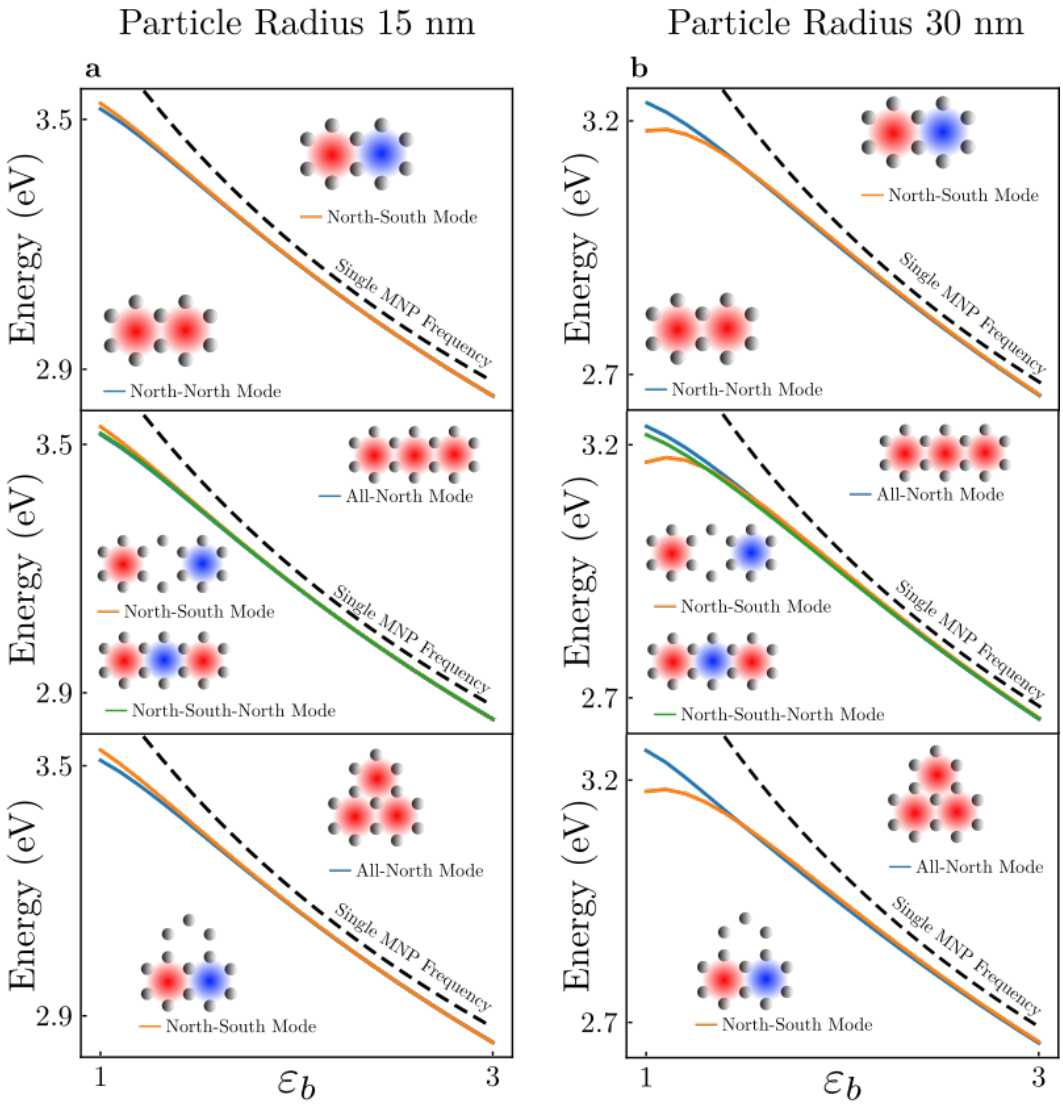

Figure 2: Magnetic mode eigenvalues for twomers (first row), threemer chains (second row), and threemer rings (third row) with particle sizes of 15 nm (column a) and 30 nm (column b) as a func tion of the dielectric constant of an embedding medium. As the dielectric constant is increased from 1 to 3, the magnetic mode splitting decreases and the overall energy decreases. At very hi gh dielectric values, the magnetic mode eigenvalues converge to the single particle resonance frequency. This can be explained by the increasing opacity of the medium effectively screening in ter-particle interactions. It is also important to note that between $\varepsilon_b = 1$ and $\varepsilon_b = 1.5$, the magnetic modes flip order. Thus, the increasing opacity of the medium e ffectively decreases the scale of the system.

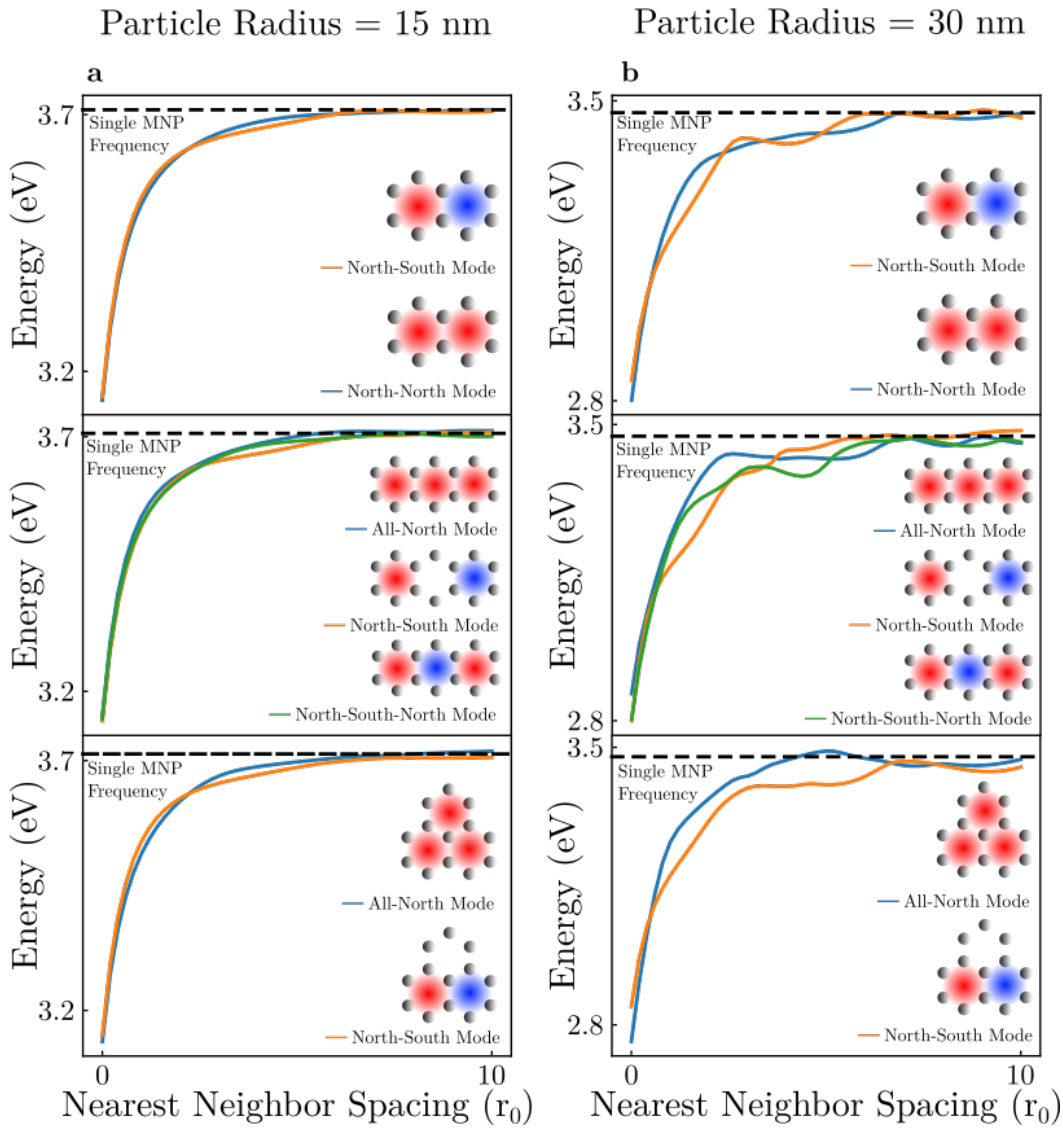

Figure 3: Magnetic mode eigenvalues for twomers (first row), threemer chains (second row), and threemer rings (third row) with particle sizes of 15 nm (column a) and 30 nm (column b) as a func tion of nearest neighbor particle spearation. The separation is plotted as a function of the particle size, in units of radii. It is important to note that as the separation distance increase s, the magnetic modes cross multiple times and their eigenvalues converge to, and oscillate about the single particle frequency. This is a result of the decreasing interaction strength. In th e limit of particles infinitely far away from each other, their interaction stength is zero. The oscillating nature of the eigenvalues is a result of the complex exponential dependence of the fields.

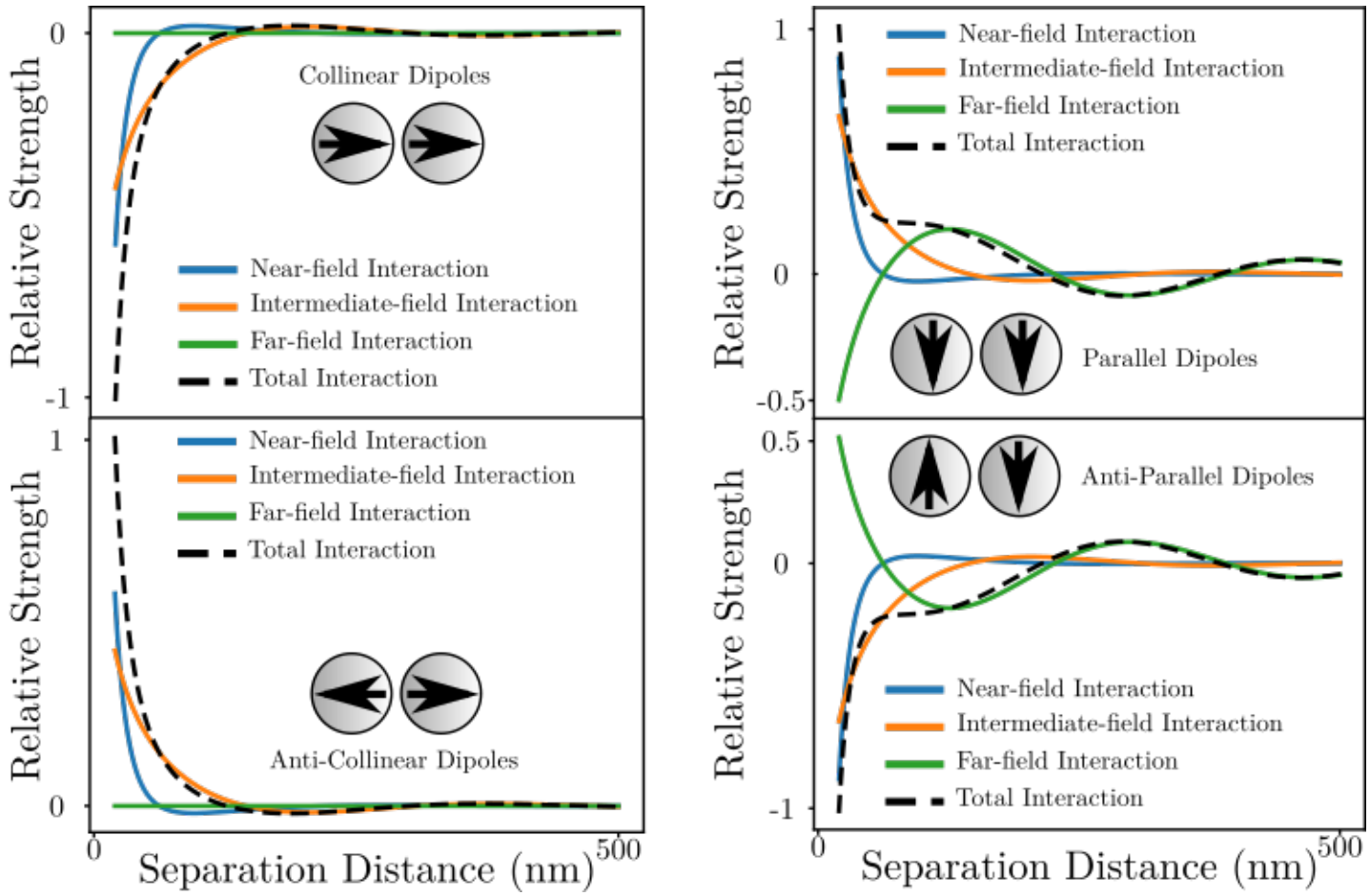

Figure 4: Relative interaction strengths for the four possible dipole arrangements of a nanoparticle dimer: collinear (a), parallel (b), anti-collinear (c), and anti-parallel (d). Plotted are the near-field (blue), intermediate-field (orange), far-field (green), and total (black, dashed) interaction strengths for each set of dipoles as a function of dipole-dipole distance. Interes tingly, and stemming from the form of the dipole relay tensor, the far-field interaction term is zero for both pairs of linear dipoles. From these plots, it can be seen that the favorability of a specific dipole arrangement depends on the separation between the dipoles. This can be seen in the fact that each part of the field depends differently on the separation, and each field term contains an oscillating term. At short length scales, the interaction is dominated by the near-field. However, as the distance increases, the interaction is dominated by the intermediate -field (a and c) or the far-field (b and d). As a result, there are separation distances at which normally unfavorable arrangements become favorable. Since magnetic oligomers can be describe through pairwise interactions of electric dipoles, it follows that the eigenvalues must also change order as different arrangements of electric dipoles become more and less favorable.

The results of our theoretical calculations and full-wave simulations for the aforementioned oligomers are dispayed in Figure **??**. Both theory and simulation predict that as a function of size, the energy ordering of the magnetic plasmon modes should change. In the two-mer system, there are two magnetic modes. When the system is small, the lowest energy mode is the alternating north-south (NS) mode and the in-phase north-north mode is highest. When we add a ring to the system, we see a trend emerge. The alternating (NSN) mode is lower than the N-S mode, which is in turn lower than the NNN mode. As a function of size, the modes change order. The triangle system, as a result of its threefold symmetry (as opposed to twofold for the chains) has slightly different properties. At small size, its lowest energy mode is a pair of degenerate NS modes, while its higher energy mode is an all-north mode. These again switch order as a function of size. In chains with more than three rings, the pattern continues - the magnetic resonances with the most nodes between rings are the lowest energy when small, but the highest when large.

This is an unexpected phenomenon. When one considers the energy-order of the four (six) hybridized modes of the nanosphere dimer, it becomes clear that they do not exhibit this effect (Figure **??**). Notably, the sphere dimer shows no crossings while the oligomer dimer does. The reason for this outcome is the oligomer dimer's complex structure.[22] The sphere dimer has only one length scale and consitutes only one pairwise interaction. However, the oligomer dimer contains many pairs of nanoparticles over multiple length scales. As a result, different configurations of electric dipoles will be favored at different oligomer sizes, hence the flip of the magnetic modes.

To gain a more visual and intuitive sense of the length scales of each of the terms (near, intermediate, and far) in the fully retarded electric field of a dipole (found in the coupling terms of Equation 2), we calculated the relative interaction strength between pairs of dipoles (the collective modes of the sphere dimer) as a function of dipole separation distance. The results of these calculations are displayed in Figure **??**, showing that at different length scales, different terms in the field contribute more to the energy of the system. Significantly, the

interaction strengths display oscillatory motion, which confirms and reinforces past studies on the oscillatory nature of radiation damping.[11]

With a functional and accurate electric dipole tight binding model, we seek a way to simplify our model. Figure **??** displays the eigenvalue curves for three arrangements of two-ring systems, with the rings as (A) nearest neighbors (B) next-nearest neighbors and (C) next-next-nearest neighbors. It is clear that again, at different length scales and relative orientations, the eigenvalue curves behave differently, having different crossing points and energy ordering. Using these eigenvalue curves, the electric dipole model is transformed into a magnetic dipole model. A magnetic dipole is placed at the center of each ring with orientation perpendicular to the plane of the ring. Each dipole has natural frequency ω_{M}, which we determine using the electric tight-binding model for a single ring. The coupling between each magnetic dipole is pulled from the plots in Figure **??** - depending on the spacing between the rings, the dipoles couple through nearest, next-nearest, or next-next-nearest neighbor coupling. The Hamiltonian

$$H = \frac{\hbar\omega_{\mathrm{M}}}{2}\sum_{i}^{n}[\pi_i^2 + q_i^2] + \frac{\hbar\omega_{\mathrm{M}}}{2}\sum_{i\neq j} g_{ij}^{\mathrm{M}} q_i q_j \tag{3}$$

is used in the same way as Equation 2 - diagonalizing it for a set of n magnetic dipoles produces n collective magnetic modes. The benefit of this model is shown by example. For the two-mer, there are ten MNPs, each with two electric dipoles, resulting in twenty collectivel electric modes, two of which were magnetic in character. In the magnetic dipole basis, because there are two rings, there are only two modes - the magnetic modes. This simplifies the data analysis procedures greatly. We find that when the couplings between rings are parametrized by the differences between the eigenvalues of the dimers in Figure **??**, the magnetic dipole Hamiltonian reproduces the results of the electric dipole Hamiltonian exactly. We find, furthermore, that truncating to nearest or next-nearest neighbors in the magnetic dipole model does not lead to any significant loss in quantitative or qualitative agreement between the models. It is this finding that will allow us the extension of the

model to larger systems considering only nearest or next-nearest neigbor coupling.

The significant challenge here is to find a colloquial, qualitative, and accurate way to describe extended systems. By considering the magnetic two-mer to be a unit cell of extended systems, the path to characterizing large systems is through a method similar to a two-atom basis molecular tight-binding model. Here, however, the atoms are the rings of the two-mer, and the elements of the hopping matrix are determined by the inter-ring couplings calculated above. More on this model will be presented later.

3 Dielectric Background

As an additional exercise, and to emphasize the tunability and versatility of magnetic plasmon oligomers, the effect of the dielectric constant of the background (ε_b) is also taken into account. The dielectric constant screens the electric dipoles from each other by effectively weakening their induced electric fields. This means that as ε_b gets large, intermediate and far field effects will weaken in comparison to near field contributions to the electric field. Thus, magnetic plasmon oligomers will be more likely to behave quasistatically when large. In Figure **??**A, the difference between the NN and NS modes for magnetic two-mers of four different scaling factors embedded in media with $\varepsilon_b = 1$ to 10 are presented as an example of the impact of screening on the energy ordering of magnetic modes. The results show that when highly screened, even large magnetic plasmon oligomers behave quasistatically.

To extend this to a potential application, we consider now a periodic chain of magnetic monomers - essentially a 1-D system - with only nearest neighbor coupling. When the radii of the particles in the chain are small, the lowest energy collective mode of the chain will be an all-alternating magnetic mode, and when the radii are large it will be an all in-phase magnetic mode. A way to quantify this is through a measure of net magnetization. Diagonalizing the magnetic Hamiltonian [reference the equation], summing the eigenvectors, and dividing by n (the number of rings) gives a measure of whether the system is magnetized, and this

is plotted as a function of particle radius in Figure **??**B. More importantly, the point at which the magnetization "switches on" can be controlled through the dielectric background. This gives rise to the ability of the experimentalist to directly introduce a phase-lag in an extended chain of magnetic oligomers by embedding certain segments of the chain in different materials. This is not so different from certain techniques that are being studied presently in the field[43]

4 Conclusion

It has been shown that magnetic plasmon oligomers are a highly versatile, highly tunable material. The magnetic behavior of tesselated rings of nanoparticles is dependent on size, spacing, arrangement, and environment. Equipped with an understanding of how information propagates along these materials and how to actively influence that information, we are now in a position to study large chains and arrays of magnetic plasmon oligomers. By combining these theoretical studies with existing experimental techniques, there exist ways to directly inlfuence the propagation of information in real time, leading to new applications in detection mechanisms and plamsonic information propagation. Furthermore, we have shown that extended networks of magnetic plasmon oligomers exhibit a negative index of refraction at optical frequencies. Future studies will elucidate the capabilities of materials designed using the knowledge gained in this exploration.

Acknowledgement

CEI, NSF, DOE?, Niket, some other people, probably

References

(1) Clippe, P.; Evrard, R.; Lucas, A. A. Aggregation Effect on the Infrared Absorption Spectrum of Small Ionic Crystals. *Phys. Rev. B* **1976**, *14*, 1715–1721.

(2) Aravind, P.; Nitzan, A.; Metiu, H. The Interaction between Electromagnetic Resonances and its Role in Spectroscopic Studies of Molecules Adsorbed on Colloidal Particles or Metal Spheres. *Surf. Sci.* **1981**, *110*, 189 – 204.

(3) Xu, Y. Electromagnetic Scattering by an Aggregate of Spheres. *Appl. Opt.* **1995**, *34*, 4573–4588.

(4) Mishchenko, M. I.; Mackowski, D. W.; Travis, L. D. Scattering of Light by Bispheres with Touching and Separated Components. *Appl. Opt.* **1995**, *34*, 4589–4599.

(5) Prodan, E.; Radloff, C.; Halas, N. J.; Nordlander, P. A Hybridization Model for the Plasmon Response of Complex Nanostructures. *Science* **2003**, *302*, 419–422.

(6) Prodan, E.; Nordlander, P. Plasmon hybridization in spherical nanoparticles. *J. of Chem. Phys.* **2004**, *120*, 5444–5454.

(7) Nordlander, P.; Oubre, C.; Prodan, E.; Li, K.; Stockman, M. I. Plasmon Hybridization in Nanoparticle Dimers. *Nano Letters* **2004**, *4*, 899–903.

(8) Davis, T. J.; Vernon, K. C.; Gómez, D. E. Designing plasmonic systems using optical coupling between nanoparticles. *Phys. Rev. B* **2009**, *79*, 155423.

(9) Myroshnychenko, V.; Rodriguez-Fernandez, J.; Pastoriza-Santos, I.; Funston, A. M.; Novo, C.; Mulvaney, P.; Liz-Marzan, L. M.; Garcia de Abajo, F. J. Modelling the optical response of gold nanoparticles. *Chem. Soc. Rev.* **2008**, *37*, 1792–1805.

(10) Turner, M. D.; Hossain, M. M.; Gu, M. The Effects of Retardation on Plasmon Hybridization within Metallic Nanostructures. *New J. of Phys.* **2010**, *12*, 083062.

(11) Dahmen, C.; Schmidt, B.; von Plessen, G. Radiation Damping in Metal Nanoparticle Pairs. *Nano Lett.* **2007**, *7*, 318–322, PMID: 17243751.

(12) Rechberger, W.; Hohenau, A.; Leitner, A.; Krenn, J.; Lamprecht, B.; Aussenegg, F. Optical Properties of Two Interacting Gold Nanoparticles. *Opt. Commun.* **2003**, *220*, 137 – 141.

(13) Kottmann, J. P.; Martin, O. J. F. Retardation-Induced plasmon Resonances in Coupled Nanoparticles. *Opt. Lett.* **2001**, 1096–1098.

(14) Haynes, C. L.; McFarland, A. D.; Zhao, L.; Van Duyne, R. P.; Schatz, G. C.; Gunnarsson, L.; Prikulis, J.; Kasemo, B.; Käll, M. Nanoparticle Optics: The Importance of Radiative Dipole Coupling in Two-Dimensional Nanoparticle Arrays. *J. Phys. Chem. B* **2003**, *107*, 7337–7342.

(15) Bouhelier, A.; Bachelot, R.; Im, J. S.; Wiederrecht, G. P.; Lerondel, G.; Kostcheev, S.; Royer, P. Electromagnetic Interactions in Plasmonic Nanoparticle Arrays. *J. Phys. Chem. B* **2005**, *109*, 3195–3198, PMID: 16851340.

(16) Kinnan, M. K.; Chumanov, G. Plasmon Coupling in Two-Dimensional Arrays of Silver Nanoparticles: II. Effect of the Particle Size and Interparticle Distance. *J. Phys. Chem. C* **2010**, *114*, 7496–7501.

(17) Alù, A.; Salandrino, A.; Engheta, N. Negative Effective Permeability and Left-Handed Materials at Optical Frequencies. *Opt. Express* **2006**, *14*, 1557–1567.

(18) Alù, A.; Engheta, N. Dynamical Theory of Artificial Optical Magnetism Produced by Rings of Plasmonic Nanoparticles. *Phys. Rev. B* **2008**, *78*, 085112.

(19) Hentschel, M.; Dregely, D.; Vogelgesang, R.; Giessen, H.; Liu, N. Plasmonic Oligomers: The Role of Individual Particles in Collective Behavior. *ACS Nano* **2011**, *5*, 2042–2050, PMID: 21344858.

(20) Brandl, D. W.; Mirin, N. A.; Nordlander, P. Plasmon Modes of Nanosphere Trimers and Quadrumers. *J. Phys. Chem. B* **2006**, *110*, 12302–12310.

(21) Cherqui, C.; Bigelow, N. W.; Vaschillo, A.; Goldwyn, H.; Masiello, D. J. Combined Tight-Binding and Numerical Electrodynamics Understanding of the STEM/EELS Magneto-Optical Responses of Aromatic Plasmon-Supporting Metal Oligomers. *ACS Photonics* **2014**, *1*, 1013–1024.

(22) Cherqui, C.; Wu, Y.; Li, G.; Quillin, S. C.; Busche, J. A.; Thakkar, N.; West, C. A.; Montoni, N. P.; Rack, P. D.; Camden, J. P. .; Masiello, D. J. STEM/EELS Imaging of Magnetic Hybridization in Symmetric and Symmetry-Broken Plasmon Oligomer Dimers and All-Magnetic Fano Interference. *Nano Lett.* **2016**, *16*, 6668–6676, PMID: 27673696.

(23) Shalaev, V. M. Optical negative-index metamaterials. *Nat. Photonics* **2007**, *1*, 41–48.

(24) Qian, Z.; Hastings, S. P.; Li, C.; Edward, B.; McGinn, C. K.; Engheta, N.; Fakhraai, Z.; Park, S.-J. Raspberry-like Metamolecules Exhibiting Strong Magnetic Resonances. *ACS Nano* **2015**, *9*, 1263–1270.

(25) Urzhumov, Y. A.; Shvets, G.; Fan, J. A.; Capasso, F.; Brandl, D.; Nordlander, P. Plasmonic Nanoclusters: a Path towards Negative-Index Metafluids. *Opt. Express* **2007**, *15*, 14129–14145.

(26) Graydon, O. Solar cells: Fano-enhanced performance. *Nat. Photonics* **2011**, *6*, 4.

(27) Le, K. Q.; Alu, A. Fano-Induced Solar Absorption Enhancement in Thin Organic Photovoltaic Cells. *Appl. Phys. Lett.* **2014**, *105*, 141118.

(28) Le, K. Q.; Bai, J. Enhanced Absorption Efficiency of Ultrathin Metamaterial Solar Absorbers by Plasmonic Fano Resonance. *JOSA B* **2015**, *32*, 595–600.

(29) Karaveli, S.; Zia, R. Strong Enhancement of Magnetic Dipole Emission in a Multilevel Electronic System. *Opt. Lett.* **2010**, *35*, 3318–3320.

(30) Noginova, N.; Zhu, G.; Mavy, M.; Noginov, M. Magnetic Dipole Based Systems for Probing Optical Magnetism. *J. Appl. Phys.* **2008**, *103*, 07E901.

(31) Wang, J.; Fan, C.; He, J.; Ding, P.; Liang, E.; Xue, Q. Double Fano Resonances Due to Interplay of Electric and Magnetic Plasmon Modes in Planar Plasmonic Structure with High Sensing Sensitivity. *Opt. Express* **2013**, *21*, 2236–2244.

(32) Zhu, Z.; Bai, B.; You, O.; Li, Q.; Fan, S. Fano Resonance Boosted Cascaded Optical Field Enhancement in a Plasmonic Nanoparticle-in-Cavity Nanoantenna Array and its SERS Application. *Light: Science and Applications* **2015**, *4*, e296.

(33) Lee, K.-L.; Huang, J.-B.; Chang, J.-W.; Wu, S.-H.; Wei, P.-K. Ultrasensitive Biosensors Using Enhanced Fano Resonances in Capped Gold Nanoslit Arrays. *Scientific Reports* **2015**, *5*, 8547.

(34) Wu, C.; Khanikaev, A. B.; Adato, R.; Arju, N.; Yanik, A. A.; Altug, H.; Shvets, G. Fano-Resonant Asymmetric Metamaterials for Ultrasensitive Spectroscopy and Identification of Molecular Monolayers. *Nat. Mat.* **2012**, *11*, 69–75.

(35) Cetin, A. E.; Altug, H. Fano Resonant Ring/Disk Plasmonic Nanocavities on Conducting Substrates for Advanced Biosensing. *ACS Nano* **2012**, *6*, 9989–9995.

(36) Zhang, S.; Bao, K.; Halas, N. J.; Xu, H.; Nordlander, P. Substrate-Induced Fano Resonances of a Plasmonic Nanocube: a Route to Increased-Sensitivity Localized Surface Plasmon Resonance Sensors Revealed. *Nano Lett.* **2011**, *11*, 1657–1663.

(37) Liu, H.; Genov, D. A.; Wu, D. M.; Liu, Y. M.; Steele, J. M.; Sun, C.; Zhu, S. N.; Zhang, X. Magnetic Plasmon Propagation Along a Chain of Connected Subwavelength Resonators at Infrared Frequencies. *Phys. Rev. Lett.* **2006**, *97*, 243902.

(38) Liu, N.; Mukherjee, S.; Bao, K.; Brown, L. V.; Dorfmüller, J.; Nordlander, P.; Halas, N. J. Magnetic Plasmon Formation and Propagation in Artificial Aromatic Molecules. *Nano Lett.* **2011**, *12*, 364–369.

(39) Liu, N.; Mukherjee, S.; Bao, K.; Li, Y.; Brown, L. V.; Nordlander, P.; Halas, N. J. Manipulating Magnetic Plasmon Propagation in Metallic Nanocluster Networks. *ACS Nano* **2012**, *6*, 5482–5488.

(40) Jackson, J. D. *Classical Electrodynamics*, 3rd ed.; Wiley: New York, NY, 1999.

(41) Hohenester, U.; Trügler, A. MNPBEM - A Matlab Toolbox for the Simulation of Plasmonic Nanoparticles. *Comp. Phys. Comm.* **2012**, *183*, 370 – 381.

(42) Purcell, E. M.; Pennypacker, C. R. Scattering and Absorption of Light by Nonspherical Dielectric Grains. *Astrophys. J.* **1973**, *186*, 705–714.

(43) Yang, A.; Hoang, T. B.; Dridi, M.; Deeb, C.; Mikkelson, M. H.; Schatz, G. C.; Odom, T. W. Real-time tunable lasing from plasmonic nanocavity arrays. *Nature Comm.* **2015**, *6*, 6939.

Graphical TOC Entry

Some journals require a graphical entry for the Table of Contents. This should be laid out "print ready" so that the sizing of the text is correct.
Inside the `tocentry` environment, the font used is Helvetica 8 pt, as required by *Journal of the American Chemical Society*.
The surrounding frame is 9 cm by 3.5 cm, which is the maximum permitted for *Journal of the American Chemical Society* graphical table of content entries. The box will not resize if the content is too big: instead it will overflow the edge of the box.
This box and the associated title will always be printed on a separate page at the end of the document.